Finite-size limitations on Quality Factor of guided resonance modes in 2D Photonic Crystals

Jon Olav Grepstad,[1,*,7] Martin M. Greve,[2,7] Bodil Holst,[2] Ib-Rune Johansen,[3] Olav Solgaard,[4] and Aasmund Sudbø,[5,6]

[1] *Department of Electronics and Telecommunications, Norwegian University of Science and Technology, NO-7491 Trondheim, Norway*
[2] *Department of Physics, University of Bergen, 5007 Bergen, Norway*
[3] *SINTEF ICT, Microsystems and Nanotechnology, NO-0373, Norway*
[4] *E.L. Ginzton Laboratory, Stanford University, CA-94305, USA*
[5] *University Graduate Center, NO-2027 Kjeller, Norway*
[6] *Department of Physics, University of Oslo, NO-0316, Norway*
[7] *The first two authors contributed equally*
[*] *jonolav.grepstad@sintef.no*

Abstract: High-Q guided resonance modes in two-dimensional photonic crystals, enable high field intensity in small volumes that can be exploited to realize high performance sensors. We show through simulations and experiments how the Q-factor of guided resonance modes varies with the size of the photonic crystal, and that this variation is due to loss caused by scattering of in-plane propagating modes at the lattice boundary and coupling of incident light to fully guided modes that exist in the homogeneous slab outside the lattice boundary. A photonic crystal with reflecting boundaries, realized by Bragg mirrors with a band gap for in-plane propagating modes, has been designed to suppress these edge effects. The new design represents a way around the fundamental limitation on Q-factors for guided resonances in finite photonic crystals. Results are presented for both simulated and fabricated structures.

OCIS codes: (220.0220) Optical design and fabrication; (280.4788) Optical sensing and sensors; (050.5298) Photonic crystals; (140.4780) Optical resonators.

References and links

1. R. Magnusson and S. S. Wang, "New principle for optical filters," Appl. Phys. Lett. **61**, 1022–1024 (1992).
2. D. Rosenblatt, A. Sharon, and A. A. Friesem, "Resonant grating waveguide structures," IEEE J. Quantum Electron. **33**, 2038–2059 (1997).
3. S. Fan and J. D. Joannopoulos, "Analysis of guided resonances in photonic crystal slabs," Phys. Rev. B **65**, 235112 (2002).
4. K. B. Crozier, V. Lousse, O. Kilic, S. Kim, S. Fan, and O. Solgaard, "Air-bridged photonic crystal slabs at visible and near-infrared wavelengths," Phys. Rev. B **73**, 115126 (2006).
5. Y. Zhou, M. C. Y. Huang, C. Chase, V. Karagodsky, M. Moewe, B. Pesala, F. G. Sedgwick, and C. J. Chang-Hasnain, "High-index-contrast grating (hcg) and its applications in optoelectronic devices," IEEE J. Sel. Top. Quantum Electron. **15**, 1485–1499 (2009).
6. C. Chase, Y. Rao, W. Hofmann, and C.-J. Chang-Hasnain, "1550 nm high contrast grating vcsel," Opt. Express **18**, 15461–15466 (2010).
7. W. Hofmann, "Evolution of high-speed long-wavelength vertical-cavity surface-emitting lasers," Semicond. Sci. Technol. **26**, 014011 (2011).

#193105 - $15.00 USD Received 1 Jul 2013; revised 28 Aug 2013; accepted 15 Sep 2013; published 27 Sep 2013

8. B. Park, J. Provine, I. W. Jung, R. T. Howe, and O. Solgaard, "Photonic crystal fiber tip sensor for high-temperature measurement," IEEE Sens. J. **11**, 2643–2648 (2011).
9. O. C. Akkaya, O. Akkaya, M. J. F. Digonnet, G. S. Kino, and O. Solgaard, "Modeling and demonstration of thermally stable high-sensitivity reproducible acoustic sensors," J. Microelectromech. Syst. **21**, 1347–1356 (2012).
10. J. O. Grepstad, P. Kaspar, O. Solgaard, I.-R. Johansen, and A. S. Sudbø, "Photonic-crystal membranes for optical detection of single nano-particles, designed for biosensor application," Opt. Express **20**, 7954–7965 (2012).
11. B. T. Cunningham and R. C. Zangar, "Photonic crystal enhanced fluorescence for early breast cancer biomarker detection," J. Biophotonics **5**, 617–628 (2012).
12. S. Fan, W. Suh, and J. D. Joannopoulos, "Temporal coupled-mode theory for the Fano resonance in optical resonators," J. Opt. Soc. Am. A **20**, 569–572 (2003).
13. W. Suh, Z. Wang, and S. Fan, "Temporal coupled-mode theory and the presence of non-orthogonal modes in lossless multimode cavities," IEEE J. Quantum Electron. **40**, 1511–1518 (2004).
14. R. R. Boye and R. K. Kostuk, "Investigation of the effect of finite grating size on the performance of guided-mode resonance filters," Appl. Opt. **39**, 3649–3653 (2000).
15. D. K. Jacob, S. C. Dunn, and M. G. Moharam, "Design considerations for narrow-band dielectric resonant grating reflection filters of finite length," J. Opt. Soc. Am. A **17**, 1241–1249 (2000).
16. J. M. Bendickson, E. N. Glytsis, T. K. Gaylord, and D. L. Brundrett, "Guided-mode resonant subwavelength gratings: effects of finite beams and finite gratings," J. Opt. Soc. Am. A **18**, 1912–1928 (2001).
17. J. Lee, B. Zhen, S.-L. Chua, W. Qiu, J. D. Joannopoulos, M. Soljacic, and O. Shapira, "Observation and differentiation of unique high-q optical resonances near zero wave vector in macroscopic photonic crystal slabs," Phys. Rev. Lett. **109**, 067401 (2012).
18. S. Ura, S. Murata, Y. Awatsuji, and K. Kintaka, "Design of resonance grating coupler," Opt. Express **16**, 12207–12213 (2008).
19. Y. Zhou, M. Moewe, J. Kern, M. C. Huang, and C. J. Chang-Hasnain, "Surface-normal emission of a high-q resonator using a subwavelength high-contrast grating," Opt. Express **16**, 17282–17287 (2008).
20. K. Kintaka, T. Majima, J. Inoue, K. Hatanaka, J. Nishii, and S. Ura, "Cavity-resonator-integrated guided-mode resonance filter for aperture miniaturization," Opt. Express **20**, 1444–1449 (2012).
21. N. C. Lindquist, A. Lesuffleur, and S.-H. Oh, "Periodic modulation of extraordinary optical transmission through subwavelength hole arrays using surrounding bragg mirrors," Phys. Rev. B **76**, 155109 (2007).
22. S.-H. Kwon, S. Kim, S.-K. Kim, Y.-H. Lee, and S.-B. Kim, "Small, low-loss heterogeneous photonic bandedge laser," Opt. Express **12**, 5356–5361 (2004).
23. P. Nedel, X. Letartre, C. Seassal, A. Auffeves, L. Ferrier, E. Drouard, A. Rahmani, and P. Viktorovitch, "Design and investigation of surface addressable photonic crystal cavity confined band edge modes for quantum photonic devices," Opt. Express **19**, 5014–5025 (2011).
24. K. Kintaka, T. Majima, K. Hatanaka, J. Inoue, and S. Ura, "Polarization-independent guided-mode resonance filter with cross-integrated waveguide resonators," Opt. Lett. **37**, 3264–3266 (2012).
25. P. Viktorovitch, B. Ben Bakir, S. Boutami, J. L. Leclercq, X. Letartre, P. Rojo-Romeo, C. Seassal, M. Zussy, L. Di Cioccio, and J. Fedeli, "3d harnessing of light with 2.5d photonic crystals," Laser Photon. Rev. **4**, 401–413 (2010).
26. J. D. Joannopoulos and S. Johnson, *Photonic Crystals, Molding the Flow of Light Second Edition* (Princeton University Press, 2008). Chapters 5 and 10.
27. T. Ochiai and K. Sakoda, "Dispersion relation and optical transmittance of a hexagonal photonic crystal slab," Phys. Rev. B **63**, 125107 (2001).
28. X. Letartre, J. Mouette, J. L. Leclercq, P. R. Romeo, c. Seassal, and P. Viktorovitch, "Switching devices with spatial and spectral resolution combining photonic crystal and moems structures," J. Lightwave Technol. **21**, 1691 (2003).
29. J.-P. Berenger, "Numerical reflection from fdtd-pmls: a comparison of the split pml with the unsplit and cfs pmls," IEEE Trans. Antennas Propag. **50**, 258–265 (2002).
30. J. O. Grepstad, M. Greve, T. Reisinger, and B. Holst, "Nano-structuring on free-standing, dielectric membranes using e-beam lithography," J. Vac. Sci. and Tech. B **31**, 06F402 (2013).

1. Introduction

Periodic permittivity induced in a layer of high index material sandwiched between two lower index materials can support a group of optical modes called guided resonance modes [1–4]. These modes are similar to fully guided modes in terms of the distribution of the mode field inside the slab, but different in that they are not fully confined to the slab. Incoming light, with a real out-of-plane k-vector, can couple to in-plane propagating modes. This gives rise to properties that are useful in applications like vertically emitting light diodes [5–7], compact narrow fiber tip sensors [8,9] and highly sensitive optical sensors for environmental control and

#193105 - $15.00 USD Received 1 Jul 2013; revised 28 Aug 2013; accepted 15 Sep 2013; published 27 Sep 2013

medical diagnosis [10, 11].

Guided resonance modes are supported in structures with both 1D- and 2D-periodic permittivity in the plane, and are qualitatively well understood by temporal coupled mode theory [12, 13]: When incoming light hits the surface of a photonic crystal (PC), it sees a combination of a homogeneous slab and an optical resonator. Part of the light is reflected and transmitted through the slab as if it was homogeneous with some effective permittivity, and is often referred to as the direct path. Another part is coupled into in-plane propagating modes that form an optical resonator associated with a resonance frequency and spectral bandwidth. The output of the resonator is referred to as the indirect path. The two paths interfere to form the characteristic Fano-shape features in the transmitted and reflected spectrum.

We present an investigation of guided resonance modes in PCs that have a 2D-periodic permittivity imposed on a dielectric slab free-standing in air, and will focus on finite-size lattice effects. Finite-size lattice effects are seldom discussed in the literature for 2D-PCs, but based on work done on 1D-PCs [14–16], we know that they can be important. Especially narrow banded guided resonance modes, i.e. high Q-factor modes, supported by PCs made in low permittivity dielectrics like Si_3N_4 and SiO_2, may not be observable if the number of periods in the lattice is too small [17]. Although simulations on infinite 2D-PCs predict that they can be used to make outstanding optical resonators with virtually unlimited Q-factor [3], there are practical limitations: The required number of unit cells can be challenging to fabricate with high enough accuracy.

Limits on the Q-factor of guided resonance modes in finite PCs are imposed by loss. Two loss mechanisms are unavoidable, even in a perfectly fabricated crystal made in a lossless dielectric. In a finite lattice, incident light will couple into in-plane propagating modes by scattering caused by the inhomogeneous permittivity in every unit cell. If the scattered light reaches the boundary of the lattice, it will see a discontinuous transition to a homogeneous slab supporting fully guided modes. Light coupled into these fully guided modes or scattered by the discontinuity, will no longer interact with the lattice and can be regarded as lost. The band diagram of an infinite PC can in many cases be used to quantify and tailor these effects [28]. For example, the in-plane group velocity of a guided resonance mode can be designed to be close to zero within a range of in-plane k-vectors. A focused incident beam can always be represented by a superposition of plane waves with a range of in-plane k-vectors. If the group velocity is small for all the plane wave components of the beam, incident light will tend not to travel far away from where it enters the slab, but be locally confined and lead to limited edge losses. Such approaches are especially useful for high-contrast gratings, where the band diagram of the infinite lattice yields the transmission spectrum for a PC with a limited number of periods in the lattice. However, for a PC composed of very weak scatterers, an unpractically large number of unit cells can be required for the band diagram of the infinite lattice to yield the transmission spectrum. In that case, the PC should be regarded as finite, and will typically exhibit higher edge losses than predicted by calculations on infinite lattices.

In order for a finite weakly scattering 2D-PC to have properties similarly to an infinite crystal, we hence have to suppress edge-loss effects. Techniques for doing so have previously been utilized to create high-Q guided-mode resonance filters with limited aperture in 1D-PCs [18–20]. They closely resemble methods to increase the transmission through metallic hole arrays supporting surface plasmon modes [21]. By placing in-plane Bragg mirrors at two of the sides of a 1D-PC cavity, light coupled to in-plane propagating guided resonance modes, can be reflected back at the lattice boundary. Incident light cannot couple to fully guided modes outside the boundaries of the lattice, making the PC work as if it was much larger than its physical size. In this way, a fundamental problem with high-Q guided resonance modes in PCs is solved, enabling performance predicted by simulations on infinite structures to be realized in finite

#193105 - $15.00 USD Received 1 Jul 2013; revised 28 Aug 2013; accepted 15 Sep 2013; published 27 Sep 2013

structures. Furthermore, fabricating a device free of defects is easier when the structured area is small. This solution can hence increase the performance of PCs in general.

It has been reported that the same principles can be applied on 2D-PCs. Lattices composed of a cavity with larger holes surrounded by smaller, have been used for lateral confinement of guided resonance modes to increase the light extraction efficiency and tailor the geometry of the output of infrared surface emitting diodes [22, 23]. Recently also an optical filter was made by utilizing a limited aperture 2D-diffraction grating bound by four Bragg mirrors [24]. We present a 2D-PC optical filter for visible light composed of a square lattice of holes etched through a free-standing dielectric membrane bound by two in-plane Bragg mirrors. Our solution is different from the work published in [24] in that our PC is not a weak grating coupling to an underlaying homogeneous waveguide. The grating and the waveguide is one and the same in our design, and is free-standing in air. We also do not have Bragg mirrors on all four sides of the PC, and show how the orientation of the Bragg-mirrors, and the number of mirrors needed, is mode dependent. This particular design of the experiment gives a novel intuitive example of how guided resonance modes behave in real finite structures.

We start by explaining how a finite PC differs from an infinite PC. We present results from simulations on finite PC lattices, which show how Fano-lines in transmission disappear when the number of holes in the crystal is too small. Next, we present simulations of our Bragg mirror PC structure, and finally show how simulated results can be reproduced in fabricated devices.

2. Guided resonance modes in finite size photonic crystals

Temporal coupled mode theory applied to PCs usually treat the case of a lossless optical resonator [3,13]. It can be modified to include loss [17,25]. For a PC free-standing in air, symmetric about the center plane, the equations used to fit a Fano-line in the transmitted and reflected spectrum is then given by

$$r = r_d \pm r_g = r_d(\omega) \pm f\frac{\gamma}{i(\omega-\omega_0)+\gamma}, \text{ and} \tag{1}$$

$$t = t_d + t_g = t_d(\omega) + f\frac{\gamma}{i(\omega-\omega_0)+\gamma}, \tag{2}$$

where ω is the frequency of the incident light, and ω_0 and γ is the center frequency and bandwidth of the guided resonance mode. The direct path is represented by reflection and transmission coefficients r_d and t_d, and the indirect path is represented by coefficients r_g and t_g.

These equations have the exact same form as a lossless optical resonator, only f is no longer set by energy conservation to be $f = -(t_d \pm r_d)$ [3]. Instead

$$f = -\alpha(t_d \pm r_d), \tag{3}$$

where α is a loss dependent scalar smaller than one. The loss can be defined to include the effect of lattice discrepancies, material absorption, etc. We will limit our discussion to loss related to edge effects, which cannot be removed by improved fabrication techniques or improved intrinsic material properties. The main differences between an infinite and a finite PC can then be illustrated as shown in Fig. 1. Figure 1(a) is the lumped element model of an infinite PC, while a finite PC is modeled in Fig. 1(b). The lossy resonator model is greatly simplified, but illustrates the point we want to make: The amplitude of the resonant term is reduced when the resonator is lossy.

The difference between an infinite and a finite lattice is especially evident when it is designed to support high-Q guided resonance modes. To understand why, we start by explaining how a PC composed of a matrix of weakly scattering holes supports high-Q guided resonance modes.

#193105 - $15.00 USD Received 1 Jul 2013; revised 28 Aug 2013; accepted 15 Sep 2013; published 27 Sep 2013

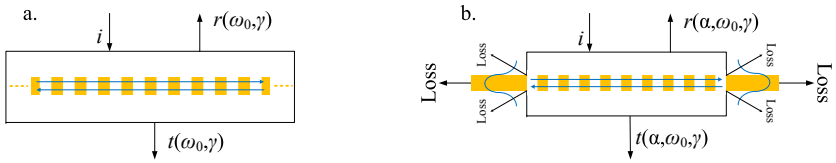

Fig. 1. (a) Lumped element model, based on temporal coupled mode theory, of an infinite photonic crystal with lattice period $p < \lambda$, where λ is the wavelength of an incoming plane wave with amplitude $i = 1$, producing a reflected and transmitted plane wave with amplitude r and t. Coupling to guided resonance modes is associated with a center frequency ω_0 and bandwidth γ. (b) Illustration of how the theory is modified to include loss related to edge effects, given by α.

Consider an infinite PC composed of unit cells with approximately homogeneous permittivity, e.g. a square lattice of holes with period p and a radius $r << p$. We also have $r << \lambda$, where λ is the wavelength of the incident field, which we choose to have normal incidence. Referring to temporal coupled mode theory, the direct response will then be approximately that of a homogeneous slab with effective permittivity slightly lower than the slab material. The resonant term is a result of incident light being scattered by the matrix of holes and coupling to a standing wave composed of waves traveling in the plane of the slab. The standing wave is similar to a sum of fully guided modes, but can scatter out of the slab by the hole matrix. This generates an out-of-plane reflected and transmitted wave. The size of the coupling coefficient, determining how much light is coupled in and out of the resonator, is hence set by the scattering strength of our hole matrix. Reducing the radius of holes, reduces the coupling coefficient. Because the Q-factor of an optical resonator is increased when the coupling coefficient is reduced, small holes or any weak scattering matrix, will generally support high-Q guided resonance modes.

The approximate band diagram of a weak scattering matrix can be found by using the dispersion relation of a homogeneous slab as a starting point. We will use a square lattice as an example. For k-vectors aligned with one of the crystals principal axes, it involves a folding of the dispersion relation of a homogeneous slab and opening of small band gaps at the edges of the Brillouin zones and at the Γ-point, as shown in Fig. 2(a) and 2(b) [4].

An incident plane wave is sent into this lattice from the side, as shown in Fig. 2(c) and 2(d). The incident wave is taken to be a fully guided mode with $k_i = 2\pi/p$ in the homogeneous slab, traveling in the positive x-direction. Its frequency, ω_{m}, lies between two guided resonance modes in the lattice. This means that we are in a photonic band gap [26] for in-plane propagating modes, which leads to an exponential decrease of the field amplitude as we go in the positive x-direction. Rows of holes in the y-direction function as an in-plane Bragg mirror, where the attenuation length will be increased when the radius of holes is reduced. In order to observe the effect of the in-plane band gap in a finite lattice composed of small holes, we hence need many periods. For the same reason, weakly scattering matrices supporting high-Q guided resonance modes, generally require many periods in order to be observed in finite size lattices.

We point out that it is possible to design crystals that have relatively large holes, and still support high-Q guided resonance modes that are forbidden by symmetry to couple to normally incident light [3,27]. Weak coupling to such modes can be achieved by breaking the symmetry, by changing the incident field to have an incidence angle slightly off from normal incidence [4]. However, whenever we have weak coupling between the incident light and a specific guided resonance mode of a PC, many periods of the PC are needed in order to observe the resonance in the transmission and reflection spectra [17].

In addition to the effect of lattice size on its ability to support a guided resonance mode, there is a second matter that needs to be considered. As lattices are finite in real experiments,

#193105 - $15.00 USD Received 1 Jul 2013; revised 28 Aug 2013; accepted 15 Sep 2013; published 27 Sep 2013

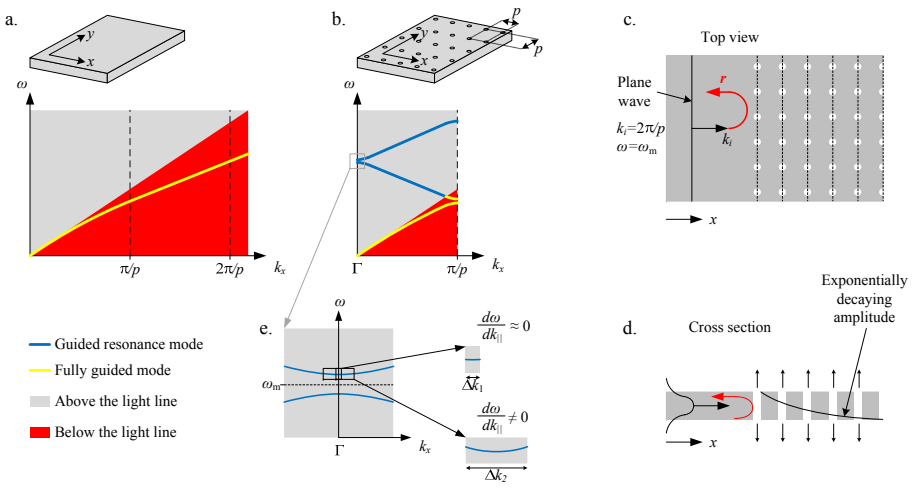

Fig. 2. (a) Dispersion relation for a homogeneous slab. (b) A square lattice of holes is introduced in the slab, which by folding about π/p introduces guided resonance modes above the light line (blue lines). A zoom-in shows the two lowest frequency guided resonance modes at the Γ-point. (c and d) We consider how a fully guided mode with frequency, ω_m, sent in from the side of this lattice, will have an exponentially decreasing amplitude as a function of distance from the lattice boundary. The decrease in amplitude is due to scattering from the holes, which creates an in-plane bad gap at this frequency. (e) Zoom in on a guided resonance mode at the Γ-point for two finite fields with different spacial extent. Going from Δk_1 to Δk_2, we go to a more localized field.

so are the incident fields. It is impossible in practice to excite a pure plane wave corresponding to a point in our band diagram. We can approximate a finite field as a sum of plane waves with different wave vectors. An incident field will hence contain a set of in-plane $k_{||}$-vectors, $\Delta k_{||}$. These sets of in-plane vectors will couple differently to a guided resonance [28]. Mathematically speaking, referring to the band diagram in Fig. 2(e) and recognizing that this plot is a projection of solutions where $k_{||} = k_x$, strong coupling requires

$$\frac{\partial \omega}{\partial k_{||}} \approx 0, \tag{4}$$

for all $k_{||}$ in $\Delta k_{||}$. If $\partial\omega/\partial k_{||} \neq 0$ for all $k_{||}$ in $\Delta k_{||}$, the transmitted and reflected spectra will be a result of coupling to a sum of guided resonance modes with different center frequency, observed as a reduction in Q-factor.

In conclusion, coupling to a guided resonance mode in finite PCs, has two main requirements. One, we have to insure that there are enough periods in our lattice for the guided resonance mode bands to form. This is closely related to the scattering strength of the lattice. Secondly, $\partial\omega/\partial k_{||}$ must be approximately zero for all in-plane k-vectors that we need in order to represent our fields.

3. Simulations on photonic crystals with finite lattices

We have designed an experiment that allows us to see how guided resonance modes disappear when the number of unit cells in a 2D-PC lattice is insufficient. We have focused on lattice size effects, since these impose fundamental limitations on the Q-factor, as oppose to finite beam size. An illustration of the simulation experiment done using FDTD is shown in Fig. 3.

#193105 - $15.00 USD Received 1 Jul 2013; revised 28 Aug 2013; accepted 15 Sep 2013; published 27 Sep 2013

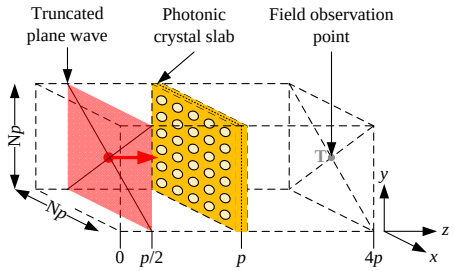

Fig. 3. Illustration of the three dimensional FDTD simulation domain. N is the number of periods in a square lattice with period p. The place of origin for the incident waves and its orientation relative to the PC, and the observation point where the field is recorded as a function time, is marked along the z-axis.

A volume, having a refractive index of air, $n_{\text{air}} = 1$, with a length corresponding to four lattice periods, $4p$, and a cross section of Np×Np, was defined. N defines the size of the lattice. The spacial resolution was set to 0.02 μm in the z-direction, and 0.01 μm in the x- and y-direction. A plane truncated wave, polarized in the y-direction, was imposed at $z = p/2$ with a Gaussian time evolution having a center frequency corresponding to $\lambda = 650$ nm in air. A slab with refractive index $n_{\text{s}} = 2$ was centered at $z = p$. The thickness of the slab was set to 160 nm and the unit cell in the lattice is composed of a hole going through the slab with a radius of 100 nm. The lattice is square with a period $p = 500$ nm.

An observation point was placed at $z = 4p$ in the center of the simulation domain on the xy-plane, allowing us to record the transmittance spectrum of the PC. Four different size lattices were simulated: N = 10, N = 20, N = 30 and an infinite lattice. N = 10, N = 20 and N = 30 were implemented by using perfectly match layers (PML) on all sides of the simulation domain. The infinite lattice was simulated by defining a domain with N = 1 and using periodic boundary conditions in both x- and y-directions.

We point out that PML does not work well for waves having k-vectors parallel to the PML [29]. Implementation of such waves is known to give rise to unphysical reflections from the boundary. This effect is present in the simulations using N = 10, N = 20 and N = 30. To reduce the required computing power and time, we simplify our model of the fabricated devices as much as possible. In spite of these simplifications and the spurious reflections from the PMLs, the simulations give us valuable insight into the physics involved.

Simulation results are presented in Fig. 4(a) and show the transmittance spectra of the four different lattice sizes. The plotted curves are the ratios between the Fourier transforms of the field recorded in point T as a function of time, and the Fourier transform of the incident Gaussian pulse. We will refer to this ratio as the transmittance. Focusing on the blue curve, two dips in transmittance can be seen. These are a result of coupling to two different guided resonance modes in the infinite lattice, and would in a simulation with higher resolution go down to zero. We will refer to the mode at 720 nm as mode A and the mode at 645 nm as mode B, as pointed out in Fig. 4(a). Note how mode A has a wider bandwidth than mode B, i.e. mode A has lower Q-factor than mode B.

In case of the finite lattice simulations, represented by the red, black and green curve, the spectrum is significantly different. We can see for both mode A and B that the resulting dips in transmission tend to disappear when the number of periods in the lattice is too small. This is clarified in Fig. 4(b), where the Q-factor of modes A and B have been calculated and plotted as a function of lattice size, represented by red and blue markers respectively. The Q-factor has been normalized as Q for the finite lattices divided by Q of the infinite lattice. The fact that

#193105 - $15.00 USD Received 1 Jul 2013; revised 28 Aug 2013; accepted 15 Sep 2013; published 27 Sep 2013

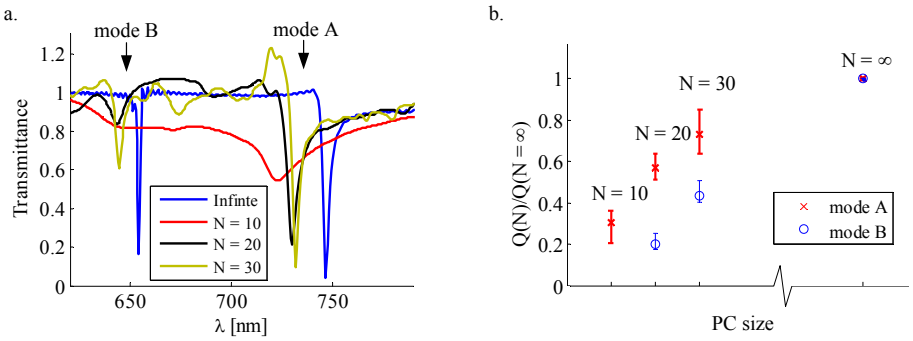

Fig. 4. (a) Simulated transmittance spectrum of a finite crystal composed of N×N holes for N = 10 (red line), N = 20 (black line), N = 30 (green line), and an infinite lattice (blue line). The transmittance is given as the ratio between the Fourier transforms of the field recorded in point T (see Fig. 3) as a function of time, and the Fourier transform of the incident pulse. Dips in transmission marked with arrows resulting from coupling to two guided resonance modes are visible, labeled mode A and B. (b) The Q-factor of mode A (red markers) and B (blue markers) has been calculated and plotted as a function of lattice size. The Q-factor has been normalized as Q for the finite lattices divided by Q of the infinite lattice.

high-Q guided resonance modes require more periods in order to be observed, can be seen by comparing the red and blue data series. Mode B is not observable for the smallest 10x10 lattice, and the Q-factor of mode A reaches its terminal value faster than mode B.

The spectra have regions in wavelength where the transmittance is above one, and there is a red shift going from small to larger lattices sizes. Values higher than one are caused by a combination of diffraction and that we are calculating the transmission based on the field amplitude at a point instead of calculating the total transmission. The red shift is caused by a reduction of $\Delta k_{||}$ as we increase the size of the lattice, in combination with band bending. As explained above, this will also limit the observable Q-factor. We will return to this matter in the discussion, to see how we can conclude that the Q-factor is mainly limited by the lattice size.

Continuous wave simulations where performed for the minima located between 700 and 750 nm in Fig. 4(a), for N = 10, N = 20 and the infinite lattice. Referring to Fig. 3, an observation plane was imposed at $z = p$, allowing us to record the field at the center of the slab. Figure 5 shows the amplitude of all three field components at this surface. The incident field is still polarized in the y-direction. From these full field images, it is evident that the sources of error mentioned earlier affect our results. Forbidden asymmetries are especially visible in the x-component of the field for the infinite lattice: The x-component of the field, shown in the bottom left in Fig. 5, does not have four folded symmetry. We can however still clearly see the underlying correct symmetric behavior of the field, and can use the results to see how the guided resonance mode is affected when making the lattice finite. Simulations with higher grid resolution were done for the 10×10 lattice. They showed that insufficient resolution is the dominant cause of these asymmetries. Effects of spurious reflections from the PML were too small to be specifically detected.

Mode A is dominated by a strong y-component, and forms as rows of holes parallel to the incident polarization oscillate in phase and couple to a guided resonance mode with in-plane k-vectors parallel to the x-axis. These are waves traveling in the positive and negative x-direction if the incident field is polarized in the y-direction. As long as the number of periods in the y-direction is large compared to the wavelength of the guided resonance mode field, it is the number of holes in the x-direction that limits the formation of the guided resonance mode.

#193105 - $15.00 USD Received 1 Jul 2013; revised 28 Aug 2013; accepted 15 Sep 2013; published 27 Sep 2013

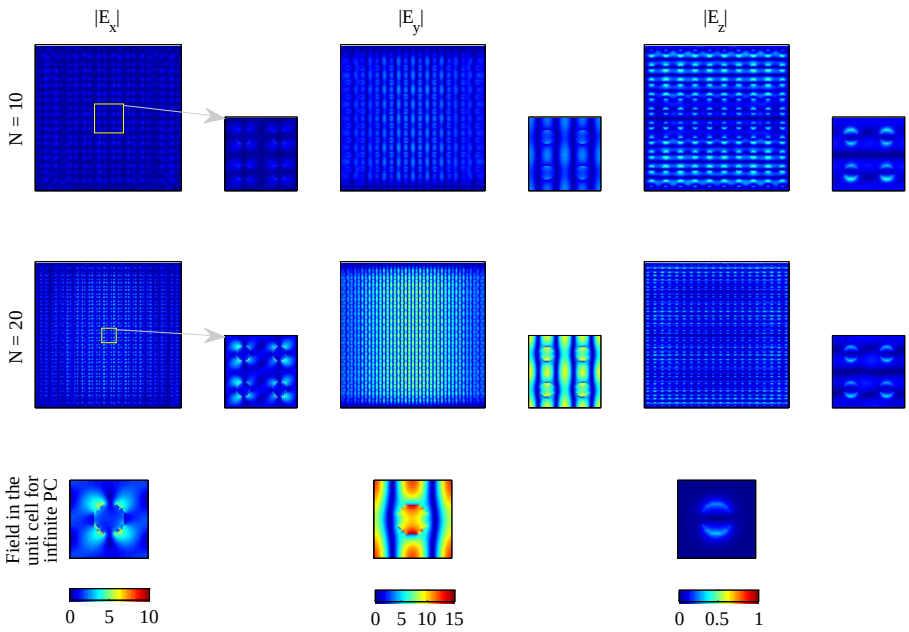

Fig. 5. Full field plots at the center plane of a finite PC consisting of 10×10 holes (N = 10) and 20×20 holes (N = 20), and the field at the center plane in a unit cell of an infinite 2D-PC, resulting from continuous wave FDTD simulations for wavelengths corresponding to the minimum values on the three plots in Fig. 4(a) above 700 nm. The center four unit cells are blown up to better see the field distribution for the two finite PCs.

Focusing on the *y*-component of the field, we can see how the field in the center of the PC converges towards the infinite case as the number of holes in the matrix increases. This is because the contribution of a specific hole to the guided resonance mode is limited in space. A unit cell at the edge, will only see the response from holes to one of its sides in the *x*-direction, while a hole in the center will see the response from neighbors on both of its sides in the *x*-direction. This causes the field in the membrane to decrease as we approach the edge of the crystal.

4. Increasing the Quality factor of finite photonic crystals

To create large Q-factors in miniaturized PC devices, we have to find a way of minimizing edge effects. A solution is to introduce reflecting boundaries. This will prevent loss induced by coupling to fully guided modes outside the lattice. For the particular mode shown in Fig. 5, this reflecting boundary condition can be imposed by placing in-plane Bragg mirrors at two of the boundaries of the lattice parallel to the incident polarization. A 3D drawing of the design is presented in Fig. 6(b). It shows a square lattice with period 500 nm, composed of holes with a radius of 100 nm imposed on a 140 nm thick membrane with refractive index $n_s = 2$. The Bragg mirrors have a period of 240 nm with open line widths of 80 nm, tuned to have an in-plane band gap for the frequency of a guided resonance mode in the hole lattice.

The transmittance spectrum of this structure is found using a setup similar to the one drawn in Fig. 3. The PC consisting only of a periodic lattice of holes, is replaced by the structure drawn in Fig. 6(b), and we simulate the response of incident fields with two orthogonal polarizations: Parallel to Bragg lines, *y*-polarized, and perpendicular to the Bragg lines, *x*-polarized. We expect

#193105 - $15.00 USD Received 1 Jul 2013; revised 28 Aug 2013; accepted 15 Sep 2013; published 27 Sep 2013

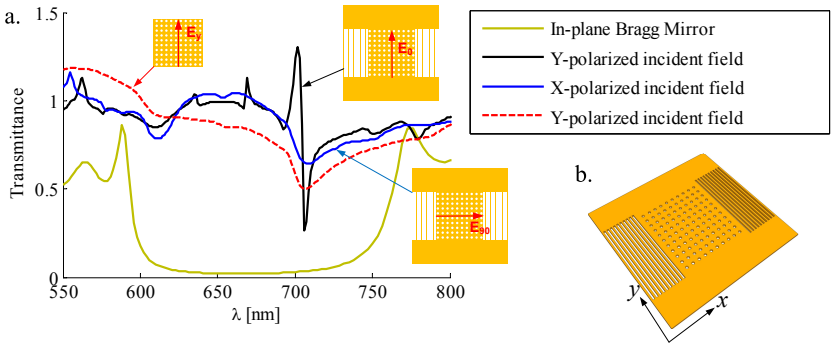

Fig. 6. (a) Simulated transmittance spectra of a PC consisting of a square lattice of 10×10 holes (red dashed), and the same hole lattice having in-plane Bragg mirrors at two of its sides. The black line results from the Bragg PC structure with incident polarization parallel to Bragg mirror lines, E_0, while the blue line results from an incident polarization perpendicular to the Bragg mirror lines, E_{90}. The transmittance is given as the ratio between the Fourier transforms of the field recorded in point T (see Fig. 3) as a function of time, and the Fourier transform of the incident pulse. The transmittance of the in-plane Bragg mirror is shown with the green line. (b) 3D illustration of the simulated PC, utilizing in-plane Bragg mirrors to trap guided resonance modes in the hole lattice with k-vectors perpendicular to the Bragg mirror lines.

that the Bragg mirrors will have little effect if the incident polarization is perpendicular to the lines in the Bragg mirror. In this case, the guided resonance mode will be waves traveling in the positive and negative y-direction. These waves do not see Bragg mirrors at the PC boundaries and can couple to fully guided modes in the homogeneous slab. For the other polarization, the guided resonance mode will be waves traveling in the positive and negative x-direction. When these waves meet the lattice boundary, they will not be allowed to propagate further and are reflected.

The results are displayed in Fig. 6(a). Four curves have been included in this plot. The in-plane Bragg mirror gives a band gap between 600 and 750 nm, as shown by the green curve. The red dashed line is the transmittance spectrum of 10×10 holes without Bragg mirrors, while the blue and black lines are the transmittance spectra of the structure in Fig. 6(b) for two different polarizations. When the polarization is perpendicular to the Bragg lines (blue line), the dip near 700 nm is clearly visible. Its minimum value is 0.65, and its width is comparable to the dip observed for the 10×10 period lattice without Bragg mirrors. Once we turn the polarization 90 degrees, a sharp dip appears that goes down to 0.13. We achieve a higher Q-factor resonance, comparable to what we see in the case of an infinite lattice. We then expect higher field amplitudes in the PC when the incident polarization is parallel to the Bragg lines. As can be seen from the continuous wave simulations presented in Fig. 7, this is the case. The figure shows the field at $z = p$ for wavelengths corresponding to the minima above 700 nm on the blue and black curves in Fig. 6(a). Referring to the center of the hole lattice, a difference in field amplitude of a factor of five can be seen when turning the incident polarization 90 degrees.

5. Fabrication and experimental setup

In order to experimentally verify the simulation results, we have fabricated PCs with dimensions similar to the ones we have simulated and characterized them optically. Due to their intended application in biosensors, the slabs are not made purely of Si_3N_4, but a more complex stack of three thin films: 50 nm Si_3N_4/50 nm SiO_2/50 nm Si_3N_4. The motive for this compo-

#193105 - $15.00 USD Received 1 Jul 2013; revised 28 Aug 2013; accepted 15 Sep 2013; published 27 Sep 2013

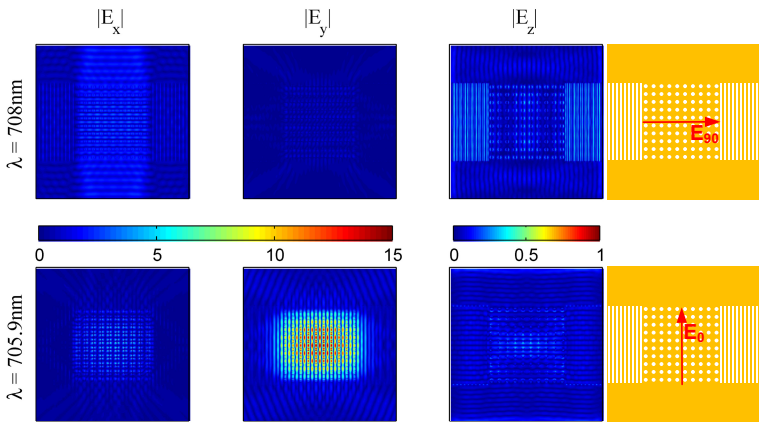

Fig. 7. Full field plots at the center plane of a PC consisting of 10×10 holes with Bragg mirrors at two of its four boundaries, for an incident field oriented perpendicular (top row) and parallel (bottom row) to the Bragg mirror lines. Plots result from continuous wave FDTD simulations for wavelengths corresponding to the minimum values of the two dips in Fig. 6(a) at 708 nm and 705.9 nm, for the incident light polarized orthogonal and parallel to the Bragg mirror lines respectively.

sition is to facilitate specific biomolecule functionalization of the PC [10]. Optically it has the effect that it lowers the effective index of the slab, because SiO_2 has lower permittivity than Si_3N_4. We expect to see similar behavior as for a pure Si_3N_4 PC, but the modes will in general be shifted towards higher frequencies. Because layers are thin compared to the operating wavelength, we do not expect to see the effect of Fabry-Perot cavities forming between boundaries of the different thin films.

First, Si_3N_4 was deposited on double side polished Si-wafers. SiO_2 was made by Poly-Si deposition followed by thermal oxidation. Standard optical lithography and a wet etch was done to form free standing membranes. Electron beam (E-beam) lithography was thereafter performed directly on the membranes to form the PC lattices. An advanced etch mask was developed to reduce charging effects and handle the fact that PMMA has poor selectivity to Si_3N_4 and SiO_2 in dry etching recipes. The mask was composed of 3 nm Cr on top of 150 nm PMMA, 20 nm SiO_2, and 150 nm polymer coating (ARC). The Cr functioned as a conductive layer during e-beam exposure of the PMMA. After e-beam exposure, the Cr was removed. The PMMA was developed, followed by a dry etch transferring the pattern into the SiO_2. Using the SiO_2 as a hard mask, the pattern was transferred to the ARC, and then into the slab. Finally, the ARC was removed. An illustration of a cross section view of a finalized chip is given in Fig. 8(f). A detailed description of the fabrication procedure can be found elsewhere [30].

Four different size PCs were made to investigate the effect of finite size lattices, composed of 10×10, 25×25, 50×50 and 100×100 periods. The final fabricated structures have a period of $p = 500 \pm 2$ nm and a hole radius of $r = 100 \pm 2$ nm. SEM images of the lattices are given in Fig. 8(a).

In the case of the PCs bound by Bragg mirrors on the sides, 2D patterns of 100 nm-radius holes with six different periods were made for a fixed set of Bragg mirror dimensions. The Bragg mirrors were made with a period of 250±2 nm and a duty cycle of 50±5 %. Four of these six designs, those with periods $p_1 = 450 \pm 2$ nm, $p_2 = 474 \pm 2$ nm, $p_3 = 500 \pm 2$ nm and $p_4 = 526 \pm 2$ nm, operated as intended. No signs of coupling to guided resonance modes was observed for periods $p_5 = 550$ nm, $p_6 = 576$ nm. The resonant modes in these structure were

#193105 - $15.00 USD Received 1 Jul 2013; revised 28 Aug 2013; accepted 15 Sep 2013; published 27 Sep 2013

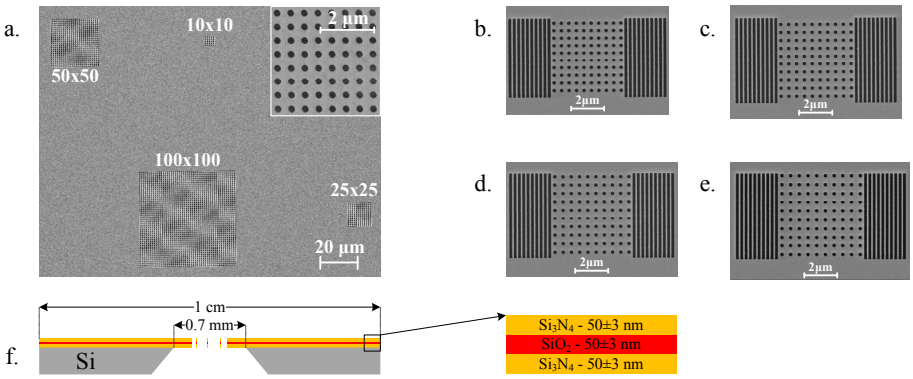

Fig. 8. Images taken with a scanning electron microscope of the fabricated structures. (a) Four square hole lattices consisting of 10×10, 25×25, 50×50 and 100×100 holes, with a period of $p = 500\pm2$ nm and a hole radius of $r = 100\pm2$ nm. (b-e) Four square hole lattices bound by in-plane Bragg mirrors. The 2D hole lattices consist of 10×10 holes, with periods (b) $p_1 = 450\pm2$ nm, (c) $p_2 = 474\pm2$ nm, (d) $p_3 = 500\pm2$ nm and (e) $p_4 = 526\pm2$ nm, from left to right. They all have a hole radius of $r = 100\pm2$ nm. The Bragg mirrors have a line spacing of 250 ± 2 nm and a duty cycle of 50 ± 5 %. All structures are etched in a 150 nm thick $Si_3N_4/SiO_2/Si_3N_4$ thin-film stack, suspended on a Si-frame. (f) Illustration of cross section view of a chip after fabrication is finalized.

outside the spectrum of our source. SEM images of the structures with p_1 to p_4 are given in Fig. 8(b)-8(e).

The optical setup measures the transmittance of the PC as a function of wavelength with spacial resolution. This is done using a 2D CCD camera connected to a Olympus BX51 Optical Microscope equipped with MPlanON 50x/0.95NA objective. A halogen lamp routed through a monochromator and a collimator provides the microscope with monochromatic backside normal incidence illumination with a bandwidth of 4.5 nm. Images were recorded with the monochromator tuned to one wavelength at a time with a spacing of 2 nm. The exposure time for each image was 5 s. The measured transmittance, presented in the results section below, is found by recording an image with and without the PC in the light path, calculating the ratio between the recorded intensities pixel by pixel.

6. Results and discussion

An image of the four different lattice sizes, as they appear in the microscope for λ=656 nm, is shown to the right in Fig. 9. Black boxes have been fitted around each lattice. The boxes are named S_{10}, S_{25}, S_{50} and S_{100}. Subscript numbers denote which lattice size each box corresponds to. A fifth box, S_0, has also been included. S_0 frames an unstructured area on the membrane. The transmittance is calculated by finding the mean value of pixels located within the boundary of each black box. The result is plotted in the graph to the left in Fig. 9.

In pixels corresponding to a solid slab, there is no sign of resonance. The 10×10 lattice, shows a broad dip around 650 nm. Looking at the plot for the 25×25 lattice, the dip close to 650 nm reaches a lower minimum value and shows a significant decrease in bandwidth. A second dip close to 570 nm also becomes visible. As we further increase the number of periods in the lattice to 50×50, these two dips continue to decrease in minimum value and bandwidth. Continuing to 100×100 periods, we do not see a decrease in minimum value, but a small increase. The bandwidth does however continue to decrease, leaving the Q-factor approximately unchanged.

#193105 - $15.00 USD Received 1 Jul 2013; revised 28 Aug 2013; accepted 15 Sep 2013; published 27 Sep 2013

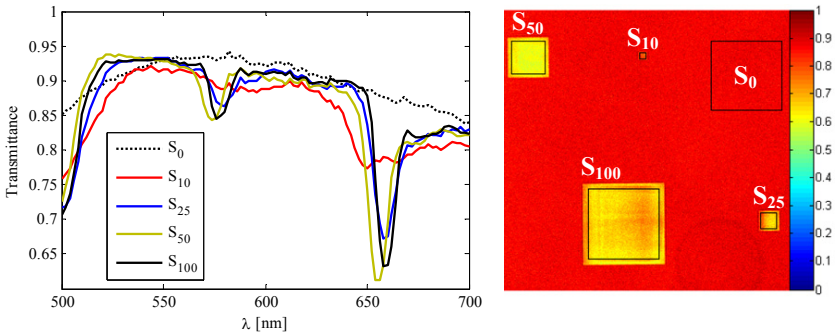

Fig. 9. (Right) Optical microscopy image of the four different lattices depicted in Fig. 8(a), recorded by a CCD camera for an incident wavelength of $\lambda = 656$ nm. Black boxes have been fitted around each lattice, named S_{10}, S_{25}, S_{50} and S_{100}. Subscripts denote the square-root of the number of holes in each lattice. A fifth box, S_0, has also been included, framing an unstructured area on the membrane. (Left) The experimentally measured transmittance, given as the mean normalized pixel value within each box, is plotted as a function of wavelength. The normalization procedure in described in section *Fabrication and experimental setup*.

The reason why we do not see a continuous increase in Q-factor and reduction of minimum dip value for larger lattice sizes than 50×50 periods, is that after 50×50 periods we start to see the effect of lattice discrepancies, such as non-symmetric holes and inhomogeneous periodicity and radius. Such defects introduce additional loss in our optical resonator model and we can hence expect a reduced Q-factor. We also note that the dip bandwidth is starting to approach the bandwidth of our scanned source for lattices larger than 50×50 periods. This limits the observable Q-factor in our optical setup. As we scan the wavelength from 500-700 nm, we do not scan a delta function over this range, but a peak with finite bandwidth of about 4.5 nm. The resulting transmittance is the convolution of the actual transmittance and source spectrum, which will also reduce the Q-factor computed directly from the transmission spectrum. In any case, the lattice size effect on guided resonance modes is clear for the three smaller lattices: As we decrease the number of holes, the effect of coupling to guided resonance modes tends to disappear.

An image of a PC with in-plane Bragg mirrors, as it appear in the microscope for $\lambda = 630$ nm (top) and 626 nm (bottom) is shown to the right in Fig. 10. SEM images have been included, showing the polarization of the incident field relative to the orientation of lines in the Bragg mirror. The period of the selected structure is $p_2 = 476$ nm, and transmittance is calculated by finding the mean value of pixels bound by each black box. The result for two orthogonal polarizations of incident light, can be seen in the graph to the left in Fig. 10.

As expected from simulations, the spectral response is highly dependent on incident polarization. When the polarization is orthogonal to lines in the Bragg mirror, a dip in reflection is visible, but the bandwidth is large and comparable to the dip seen for the 10×10 holes lattice with no Bragg mirrors in Fig. 9. Once we turn the polarization parallel to the Bragg lines, the dip bandwidth and minimum value is significantly decreased. Considering that the holes are not perfectly symmetric and the Bragg lines have a roughness in our real structures, the fabricated devices perform well and clearly show how the Q-factor of a finite PC can be increased by exploiting reflecting boundary conditions. Comparing the transmittance for different Bragg PC structures depicted in Fig. 8, dip minimum values range from 0.65 to 0.70, and the position of the dips are period dependent, but they all show the same trends.

#193105 - $15.00 USD Received 1 Jul 2013; revised 28 Aug 2013; accepted 15 Sep 2013; published 27 Sep 2013

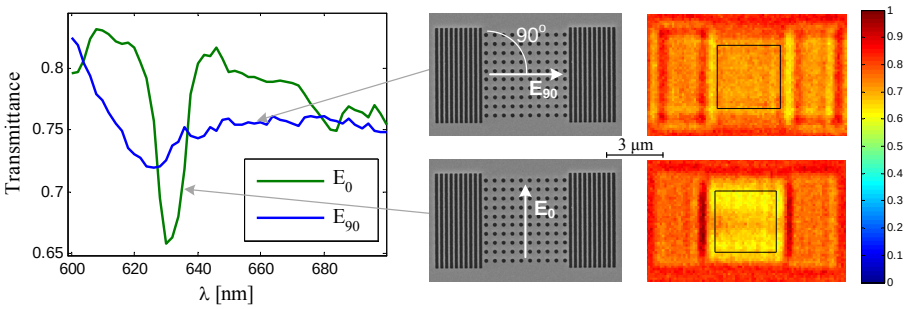

Fig. 10. (Very right) Optical microscopy images recorded with a CCD camera for two orthogonal polarizations of incident light, at wavelengths $\lambda = 630$ nm (top) and 626 nm (bottom), for the Bragg PC structure with period 476 nm (middle). (Left) The experimentally measured transmittance, given as the mean normalized pixel value within each box, is plotted as a function of wavelength. The normalization procedure in described in section *Fabrication and experimental setup*.

We note that position of the Bragg mirrors relative to the photonic crystal lattice has not been studied extensively. Light traveling in the plane, should be reflected back into the crystal as if the PC was infinite. If the phase of the reflection from the mirrors is off, we can see the opposite effect of what we are aiming for, namely weaker coupling to guided resonance modes as opposed to stronger. We also know that there will be light scattered out of the membrane at the edges, when in-plane modes meet the jump in effective index between the lattice and the homogeneous slab. Optimizing the position of the Bragg mirrors and designing a smooth transition in effective index between the lattice and the homogeneous slab, will increase the performance of our device.

We finally return to the red shift observed in Fig. 4(a) as the lattice size is increased. It is due to the fact that the bands supporting mode A and B in our structure have a positive second order derivative, $\partial^2\omega/\partial k_{||}^2 > 0$, at the Γ-point. This has been verified in simulations. Hence, as we increase the lattice size and decrease $\Delta k_{||}$, the sum of excited guided resonance modes have decreasing mean center frequency. This causes a red shift of the center wavelength of our dip in transmission, and is accompanied by an increase in observed Q-factor. The weak observable coupling to guided resonance modes in the smaller lattices, can hence be caused by excess band bending or insufficient lattice size. However, due to the strong polarization dependence evident in the Bragg PC structure, we can clearly see that the lattice size effect is dominating. This statement is further supported by inspecting the top left plot in Fig. 7. In this plot we see how there are in-plane waves propagating away from the lattice above and below the holes when the Bragg mirrors are not containing the guided resonance mode.

7. Conclusion

We have shown that guided resonance modes in 2D-PCs are not observable in the transmission spectrum of the PC if the number of periods in the lattice is insufficient. This agrees with analytic models developed for 1D-PCs [15, 16] and experimental studies of large 2D-PCs [17], and can be understood by considering a finite PC as an optical resonator with loss.

The fundamental loss mechanisms are related to coupling of incident light to fully guided modes existing outside the boundaries of the lattice and scattering of in-plane propagating waves at the lattice boundaries. We have shown how coupling to fully guided modes can be suppressed by introducing reflecting boundary conditions. This can be done using Bragg mir-

#193105 - $15.00 USD Received 1 Jul 2013; revised 28 Aug 2013; accepted 15 Sep 2013; published 27 Sep 2013

rors that have a band gap for in-plane propagating modes. Methods to reduce scattering at the lattice boundaries have not been investigated.

While our devices do not support guided resonance modes with extraordinary narrow bandwidths, the results show how lattices with limited extent can be made to work as if they are larger. Extrapolation of these results, indicate that a PC perfectly fabricated over a large number of periods can be replaced by a PC that is perfect over a small area and bound by an in-plane band gap. This is useful with respect to PCs being applied in real devices, especially in devices with high demands on miniaturization and the Q-factor of guided resonance modes.

Acknowledgment

All the photonic crystal structures used in this project were made at the University of Bergen Nanostructures Laboratory. We thank Trond Mohn, The University of Bergen and the Norwegian Research council (NFR) for funding. We also thank NFR for their support through the Norwegian PhD Network on Nanotechnology for Microsystems, IndustriPhD program and ISBILAT program.

#193105 - $15.00 USD Received 1 Jul 2013; revised 28 Aug 2013; accepted 15 Sep 2013; published 27 Sep 2013